Stress analysis of junction of plate and shell built-up structures via special finite shell element

Stress Analysis of Junction of Plate and Shell Built-Up Structures via Special Finite Shell Element*

Koetsu YAMAZAKI** and Noriaki TSUBOSAKA***

A finite element formulation using the penalty function method to analyze exactly the junction of plate and shell built-up structures is suggested for an isoparametric shell element. The connectivity condition at the junction is added to the potential energy functional by the penalty parameter and the interpolating function of displacements. This formulation yields an integral-type stiffness matrix of the special junction elements, which can directly evaluate the surface tractions at the junction. The suggested technique is applied to the stress analyses of isotropic and laminated plates with several types of stiffeners, and the validity of the technique is discussed.

Key Words: Structural Analysis, Finite Element Method, Junction Parts, Stiffened Plate Structure, Composite Laminated Plate, Penalty Method

1. Introduction

When we consider the design of built-up structures composed of plates and shells, such as stiffened plate and shell structures, it is very important and indispensible to take the stress concentration at the ends of the junction into consideration, since failures or cracks in the vicinity of the junction of such structures can be observed in practice. Generation of a numerical analysis model including such stress concentration, however, is difficult using general-use finite element codes, since the deformations of the plate and shell structures are approximated by representative nodes at the midsurface of the thin plate and shell structures and the connectivity condition at the adhered surface can not be represented exactly. It is not also expected to be able to adopt three-dimensional brick-type elements to treat the connectivity condition exactly, because such elements lead to an increase of the number of degrees of freedom.

For more exact analysis of the built-up structures with adhesion, contact analysis techniques are applicable wherein the bonded regions are regarded as being in the pseudo sticking state. There are many techniques by which to analyze contact problems[1]-[4], such as the thin film element method, Lagrange multiplier method and the penalty function method. Among them, the penalty function method[4] is one of the most efficient methods for solving the contact problems, because it does not require any increase of the number of degrees of freedom in the final equation to be solved, and the size of the coefficient matrix of the system remains the same. In the early works concerning contact analysis, the contact condition at the nodal points on the contact interface was included directly into the energy functional by the form as (penalty parameter) × (displacement difference between the corresponding nodes), which has no real physical meaning.

Therefore, in this paper we will suggest an

* Received 17th March, 1995. Japanese original : Trans. Jpn. Soc. Mech. Eng., Vol. 59, No. 568, A (1993), pp. 3041-3047. (Received 7th June, 1993)

** Department of Mechanical Systems Engineering, Kanazawa University, 2-40-20 Kodatsuno, Kanazawa 920, Japan

*** Nippon Sharyo Production Co., Ltd., 1-1 Sanbonmatsu-machi, Atsuta-ku, Nagoya 456-91, Japan

integral type of isoparametric shell connecting element to represent the connectivity condition exactly at the adhered region by the penalty function method, in which the connectivity condition at the junction will be added to the potential energy functional by the penalty parameter and interpolating function of displacements, and the finite element formulation to analyze the adhesive plate and shell structures will be derived. Then, the method suggested here will be applied for analyzing the built-up structures such as the isotropic and laminated composite plates with several kinds of stiffeners.

2. Finite Element Analysis of Built-Up Structures via Penalty Method

2.1 Derivation of formulation including connectivity condition

Let us consider the analysis of the plate and shell built-up structures shown in Fig. 1. If it is assumed that plates A and B are deformed as a whole at the junction, the adhesion condition is described by the continuity condition of displacements at the adhered surface as

$$u_{i\zeta=-1}^{A}=u_{i\zeta=-1}^{B}, \tag{1}$$

where u_i^A and u_i^B $(i=1, 2, 3)$ denote the displacement components of plates A and B in the global Cartesian coordinates, and the parametric coordinates $\zeta=\pm 1$ represent the adhered surface of the plates. By adding the adhesion condition to the conventional potential energy functional using the penalty function method, the total stiffness equation is derived from the stationary condition of the modified energy functional. If we denote the total potential energy, the internal potential and the external potential of both plates by Π, U and V, the modified potential functional can be expressed as

$$\Pi=U+V+\frac{1}{2}\alpha\int_{S_h}\sum_{i=1}^{3}(u_{i\zeta=-1}^{A}-u_{i\zeta=+1}^{B})^2dS\rightarrow\min \tag{2}$$

where α is the penalty parameter, and the integration is taken over the adhered surface S_h. The above functional includes the equality condition (1); however, the equality constraint is satisfied exactly only when the penalty parameter α tends to infinity. When the stress, strain tensors and surface traction are denoted by σ_{ij}^{β}, ε_{ij}^{β} and $f_i^{\beta}(\beta=A, B)$, the following stationary condition can be derived from Eq.(2).

$$\delta\Pi=\int_{V_A}\sigma_{ij}^{A}\delta\varepsilon_{ij}^{A}dV+\int_{V_B}\sigma_{ij}^{B}\delta\varepsilon_{ij}^{B}dV-\int_{S_A}f_i^{A}\delta u_i^{A}dS-\int_{S_B}f_i^{B}\delta u_i^{B}dS+\alpha\int_{S_h}(u_{i\zeta=-1}^{A}-u_{i\zeta=1}^{B})(\delta u_{i\zeta=-1}^{A}-\delta u_{i\zeta=1}^{B})dS=0 \tag{3}$$

Here, δ represents the variational operator, and the integration of the first and second terms requires volume integration over plates A and B. On the other hand, the integration of third and fourth terms shows surface integration.

2.2 Discretization into finite shell element

As in the conventional finite element formulation, Eq.(3) is discretized into finite elements. We will consider an isoparametric quadratic shell element with eight nodes, as shown in Fig. 2, in the following. In the isoparametric finite shell elements, the Cartesian coordinate x_i and the displacement u_i at any point $(\xi, \eta, \zeta)(-1\leq\xi, \eta, \zeta\leq 1)$ of parametric coordinates are interpolated by the same quadratic function $N_k(\xi, \eta)$ for node k as

$$\begin{Bmatrix}x_1\\x_2\\x_3\end{Bmatrix}=\sum_{k=1}^{8}N_k(\xi,\eta)\begin{Bmatrix}x_{1k}\\x_{2k}\\x_{3k}\end{Bmatrix}+\sum_{k=1}^{8}N_k(\xi,\eta)\frac{t}{2}\zeta v_{3k}, \tag{4}$$

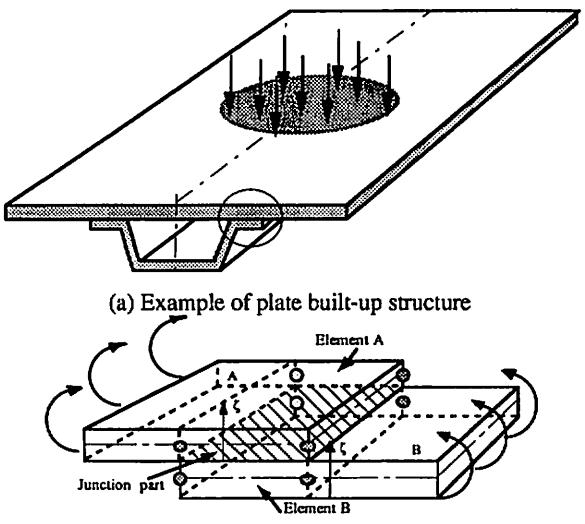

Fig. 1 Plate built-up structure and its junction

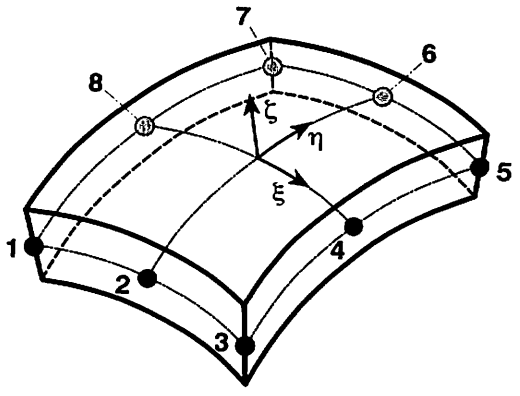

Fig. 2 Isoparametric finite shell element with eight-nodes

$$\begin{Bmatrix} u_1 \\ u_2 \\ u_3 \end{Bmatrix} = \sum_{k=1}^{8} N_k(\xi, \eta) \begin{Bmatrix} u_{1k} \\ u_{2k} \\ u_{3k} \end{Bmatrix} + \sum_{k=1}^{8} N_k(\xi, \eta) \frac{t}{2} \zeta [v_{1k}, -v_{2k}] \begin{Bmatrix} \alpha_k \\ \beta_k \end{Bmatrix}, \quad (5)$$

in which t, x_{ik} and u_{ik} are the thickness, the coordinate x_i and the displacement u_i at nodal point k in an element, and the parametric coordinate ζ refers to the direction perpendicular to the midsurface of the shell. The vector v_{3k} is a unit vector of node k in the ζ direction, and α_k and β_k denote the rotation angles around the normal unit vectors v_1 and v_2 defined perpendicular to v_3 on the midsurface of the plate.

Then, the displacements on the adhered surfaces are represented as

$$\begin{Bmatrix} u_1^A \\ u_2^A \\ u_3^A \end{Bmatrix}_{\zeta=-1} = \sum_{k=1}^{8} [C_k^A] \{d_{ek}^A\}, \quad \begin{Bmatrix} u_1^B \\ u_2^B \\ u_3^B \end{Bmatrix}_{\zeta=1} = \sum_{k=1}^{8} [C_k^B] \{d_{ek}^B\}, \quad (6)$$

in which $[C_k^A]$ and $[C_k^B]$ are the matrices relating the displacements on the adhered surface to the nodal displacement vector $\{d_{ek}^\beta\} = (u_{1k}^\beta, u_{2k}^\beta, u_{3k}^\beta, \alpha_k^\beta, \beta_k^\beta)^T (\beta = A, B)$. Using the components of normal unit vectors v_1 and v_2, the matrices $[C_k^A]$ and $[C_k^B]$ are given as

$$[C_k^A] = \begin{bmatrix} N_k & 0 & 0 & -\frac{t}{2} N_k \nu_{11}^k & \frac{t}{2} N_k \nu_{21}^k \\ 0 & N_k & 0 & -\frac{t}{2} N_k \nu_{12}^k & \frac{t}{2} N_k \nu_{22}^k \\ 0 & 0 & N_k & -\frac{t}{2} N_k \nu_{13}^k & \frac{t}{2} N_k \nu_{23}^k \end{bmatrix}$$

$$[C_k^B] = \begin{bmatrix} N_k & 0 & 0 & \frac{t}{2} N_k \nu_{11}^k & -\frac{t}{2} N_k \nu_{21}^k \\ 0 & N_k & 0 & \frac{t}{2} N_k \nu_{12}^k & -\frac{t}{2} N_k \nu_{22}^k \\ 0 & 0 & N_k & \frac{t}{2} N_k \nu_{13}^k & -\frac{t}{2} N_k \nu_{23}^k \end{bmatrix}. \quad (k = 1, 2, \cdots, 8) \quad (7)$$

By substituting Eqs.(5) and (6) into Eq.(3), the following total equilibrium equation for the built-up structures is derived.

$$\sum_{V_A}^{e} \delta\{d_e^A\}^T [K_e^A] \{d_e^A\} + \sum_{V_B}^{e} \delta\{d_e^B\}^T [K_e^B] \{d_e^B\} - \sum_{S_A}^{e} \delta\{d_e^A\}^T \{f_e^A\} - \sum_{S_B}^{e} \delta\{d_e^B\}^T \{f_e^B\} + \sum_{S_h}^{e} \{\delta\{d_e^A\}^T, \delta\{d_e^B\}^T\} [K_{he}^B] \begin{Bmatrix} \{d_e^A\} \\ \{d_e^B\} \end{Bmatrix} = 0 \quad (8)$$

where $[K_e^A]$, $[K_e^B]$ and $\{d_e^A\}$, $\{d_e^B\}$ denote the element stiffness matrices and the nodal displacement vectors of an element e in plates A and B, and $\{F_e^A\}$, $\{F_e^B\}$ represent the equivalent nodal force vectors corresponding to the surface tractions of the two plates. On the other hand, the matrix $[K_{he}]$ represents the stiffness of the connecting elements between plates A and B at the junction and the summation is taken over the special connecting elements.

2.3 Element stiffness matrix

Next, let us consider derivation of the element stiffness matrix of a laminated composite plate for application to the laminated composite built-up structures. The strain $\{\varepsilon\} = \{\varepsilon_{x'}, \varepsilon_{y'}, \gamma_{x'y'}, \gamma_{x'z'}, \gamma_{y'z'}\}^T$ in the (x', y', z') local coordinates defined by the unit vector transformation matrices $[\phi] = [v_1, v_2, v_3]$ and $[\Psi_k] = [\phi]^T [v_{1k}, -v_{2k}]$ in an element is interpolated from Eq.(5) as

$$\{\varepsilon\} = \sum_k [B_k] [\phi]^T \begin{Bmatrix} u_{1k} \\ u_{2k} \\ u_{3k} \end{Bmatrix} + \sum_k \frac{t}{2} (\zeta [B_k] + [C_k]) [\Psi]^T \begin{Bmatrix} \alpha_k \\ \beta_k \end{Bmatrix}, \quad (9)$$

where the matrices $[B_k]$ and $[C_k]$ relate the nodal displacements and the rotation angles to the strain components, and are given as

$$[B_k] = \begin{bmatrix} B_{1k} & 0 & 0 \\ 0 & B_{2k} & 0 \\ B_{2k} & B_{1k} & 0 \\ B_{3k} & 0 & B_{1k} \\ 0 & B_{3k} & B_{2k} \end{bmatrix}, \quad [C_k] = \begin{bmatrix} 0 & 0 & 0 \\ 0 & 0 & 0 \\ 0 & 0 & 0 \\ C_{3k} & 0 & 0 \\ 0 & C_{3k} & 0 \end{bmatrix}$$

$$B_{1k} = A_{11} \frac{\partial N_k}{\partial \xi} + A_{12} \frac{\partial N_k}{\partial \eta}, \quad B_{2k} = A_{21} \frac{\partial N_k}{\partial \xi} + A_{22} \frac{\partial N_k}{\partial \xi},$$

$$B_{3k} = A_{31} \frac{\partial N_k}{\partial \xi} + A_{32} \frac{\partial N_k}{\partial \eta}, \quad C_{3k} = A_{33} N_k, \quad (10)$$

in which A_{ij} are the components defined using the Jaccobian $[J]$ as

$$[A] = [\phi]^T [J]^{-1} = \begin{bmatrix} A_{11} & A_{12} & 0 \\ A_{21} & A_{22} & 0 \\ A_{31} & A_{32} & A_{33} \end{bmatrix}. \quad (11)$$

Then, symmetric layer construction with respect to the midsurface of the laminated plate is assumed. When we denote the stress and strain components in the uniaxial fiber direction and its perpendicular direction at the p-th layer, shown in Fig. 3, as $\{\sigma'\}_p = (\sigma_1, \sigma_2, \tau_{12})^T$, $\{\tau'\}_p = (\tau_{13}, \tau_{23})^T$ and $\{\varepsilon'\}_p = (\varepsilon_1, \varepsilon_2, \gamma_{12})^T$, $\{\gamma'\}_p = (\gamma_{13}, \gamma_{23})^T$, then the stress-strain relationship of a unidirectionally reinforced composite gives[5]

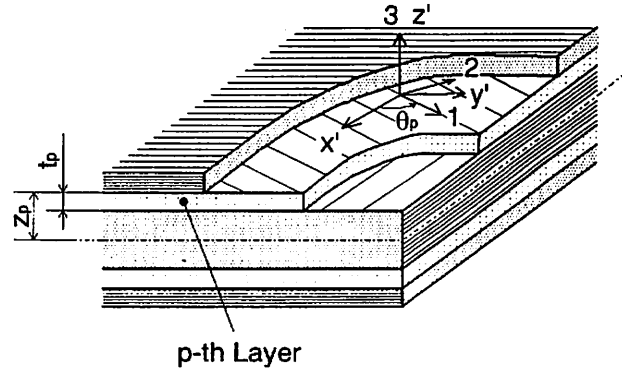

Fig. 3 Model of symmetric layer construction of laminated composite plate

$$\{\sigma'\}_p=[Q_1']\{\varepsilon'\}_p,\ \{\tau'\}_p=[Q_2']\{\gamma'\}_p, \tag{12}$$

where the stress-strain matrices are given as

$$[Q_1']=\begin{bmatrix} \frac{E_1}{1-\nu_{12}\nu_{21}} & \frac{\nu_{12}E_2}{1-\nu_{12}\nu_{21}} & 0 \\ \frac{\nu_{21}E_1}{1-\nu_{12}\nu_{21}} & \frac{E_2}{1-\nu_{12}\nu_{21}} & 0 \\ 0 & 0 & G_{12} \end{bmatrix},$$

$$[Q_2']=\begin{bmatrix} \kappa_1 G_{13} & 0 \\ 0 & \kappa_2 G_{23} \end{bmatrix}, \tag{13}$$

in which E_1, E_2 ; ν_{12}, ν_{21} ; and G_{12}, G_{13}, G_{23} represent the Young's moduli, Poisson's ratios and the shear moduli in the unidirectional composite plate. The modified coefficients of shear are taken as $\kappa_1=\kappa_2=1/1.2$ in this formulation. By transforming the stress-strain relationship(12) into the local coordinates (x', y', z'), the stress components $\{\sigma\}=\{\sigma_{x'}, \sigma_{y'}, \tau_{x'y'}, \tau_{x'z'}, \tau_{y'z'}\}^T$ in the (x', y', z') local coordinates are given as

$$\{\sigma\}_p=\begin{bmatrix} [Q_1]_p & 0 \\ 0 & [Q_2]_p \end{bmatrix}\{\varepsilon\}=[Q]_p\{\varepsilon\}, \tag{14}$$

where

$$[Q_1]_p=[T_1]_p^T[Q_1'][T_1]_p,\ [Q_2]_p=[T_2]_p^T[Q_2'][T_2]_p,$$

$$[T_1]_p=\begin{bmatrix} c^2 & s^2 & cs \\ s^2 & c^2 & -cs \\ -2cs & 2cs & c^2-s^2 \end{bmatrix},\ [T_2]_p=\begin{bmatrix} c & s \\ -s & c \end{bmatrix}, \tag{15}$$

in which $c=\cos\theta_p$ and $s=\sin\theta_p$ when the angle θ_p is the fiber direction measured from the axis x' in the counterclockwise direction, as shown in Fig. 3.

Then, the l, m component of the element stiffness matrix of a symmetric laminate is obtained from Eqs. (9) and (14) as

$$[K_{lm}]=\begin{bmatrix} K_{lm}^{11} & K_{lm}^{12} \\ K_{lm}^{21} & K_{lm}^{22} \end{bmatrix}\quad (l, m=1, 2, \cdots, 8). \tag{16}$$

Each component of the above expression is evaluated by

$$\begin{aligned}
[K_{lm}^{11}]&=2\int_{-1}^{1}\int_{-1}^{1}[\phi][B_l]^T[D_1][B_m][\phi]^T|J|d\xi d\eta \\
[K_{lm}^{12}]&=t\int_{-1}^{1}\int_{-1}^{1}[\phi][B_l]^T[D_1][C_m][\Psi]^T|J|d\xi d\eta \\
[K_{lm}^{21}]&=t\int_{-1}^{1}\int_{-1}^{1}[\Psi][C_l]^T[D_1][B_m][\phi]^T|J|d\xi d\eta \\
[K_{lm}^{22}]&=\frac{t^2}{6}\int_{-1}^{1}\int_{-1}^{1}[\phi][B_l]^T[D_2][B_m][\phi]^T|J|d\xi d\eta \\
&\quad+\frac{t^2}{2}\int_{-1}^{1}\int_{-1}^{1}[\Psi][C_l]^T[D_1][C_m][\Psi]^T|J|d\xi d\eta,
\end{aligned} \tag{17}$$

in which the stress-strain matrices $[D_1]$ and $[D_2]$ are given by the summation over the all layers $2n$ as

$$\begin{aligned}
[D_1]&=\sum_{p=1}^{n}\frac{2t_p}{t}[Q]_p, \\
[D_2]&=\sum_{p=1}^{n}\frac{8}{t^3}\{z_p^3-(z_p-t_p)^3\}[Q]_p,
\end{aligned} \tag{18}$$

where t_p and z_p denote the thickness of the p-th layer and the distance between the mid-surface and the outer surface of the p-th layer. For isotropic materials, Eqs. (12) through (18) are simplified by replacing $E_1=E_2=E$, $\nu_{12}=\nu_{21}=\nu$ and $G_{12}=G_{13}=G_{23}=G$.

2.4 Element stiffness matrix of connecting special element

The stiffness matrix of the connecting element is derived from the adhesion condition Eq. (1) and the interpolation relations of displacement of Eq. (6) as

$$[K_{he}]=\begin{bmatrix} K_h^{AA} & K_h^{AB} \\ K_h^{BA} & K_h^{BB} \end{bmatrix}, \tag{19}$$

where

$$\begin{aligned}
[K_h^{AA}]&=\alpha\int_{S_{he}}[C^A]^T[C^A]dS, \\
[K_h^{AB}]&=-\alpha\int_{S_{he}}[C^A]^T[C^B]dS \\
[K_h^{BA}]&=-\alpha\int_{S_{he}}[C^B]^T[C^A]dS, \\
[K_h^{BB}]&=\alpha\int_{S_{he}}[C^B]^T[C^B]dS,
\end{aligned} \tag{20}$$

in which α denotes the penalty parameter and the integration must be taken over the adhered surface of the connecting element. $[C_A]$ and $[C_B]$ are the matrices relating the displacements on the adhered surface to the nodal displacement vector, and consist of $[C_h^A]$ and $[C_h^B]$ defined in Eq. (7) as

$$[C^A]=[C_1^A, C_2^A, \cdots, C_8^A],\ [C^B]=[C_1^B, C_2^B, \cdots, C_8^B]. \tag{21}$$

When the element stiffness matrices are assembled to the total stiffness matrices, the total system of equations to be solved can finally be expressed as

$$\begin{bmatrix} K^A & 0 \\ 0 & K^B \end{bmatrix}\begin{Bmatrix} d^A \\ d^B \end{Bmatrix}+[K_h]\begin{Bmatrix} d^A \\ d^B \end{Bmatrix}=\begin{Bmatrix} F^A \\ F^B \end{Bmatrix}, \tag{22}$$

where $\{d^A\}$ and $\{d^B\}$ are the total nodal displacement vectors of plates A and B, and the matrix $[K_h]$ connecting $\{d^B\}$ with $\{d^A\}$ is assembled by the connecting element stiffness $[K_{he}]$ into the corresponding position of total stiffness as in the conventional manner. After solving Eq. (22) for the nodal displacement vectors, the stress recovery of each element is calculated. The components of the traction vector on the adhered surface are also evaluated from the difference in the corresponding nodal displacements as

$$f_i^A=-f_i^B=\alpha(u_{i\xi=-1}^A-u_{i\xi=1}^B). \tag{23}$$

3. Numerical Examples

The stress analysis formulation for the plate and shell built-up structures mentioned above is applied to the structural analyses of isotropic and composite plates with stiffener. The numerical examples are implemented with double precision of word length and the penalty parameter $\alpha=10^6$. The precision of the displacement and stress distributions is confirmed numerically for the isotropic bilayered plate supported at opposite sides by comparing the results for a single-layered plate with the same total thickness.

3.1 Uniform bending of simply supported srip with stiffener

For the first example, uniform bending of a simply supported strip with a T-type stiffener in the longitudinal direction is considered, as shown in Fig. 4. Because of symmetry, a quarter region of the model is subdivided into 77 elements and 283 nodes, where 21 elements cover the adhered region between the strip and the stiffener.

The center deflection ratio of this numerical model to that of beam theory with the same flexural rigidity is $w/w_{th}=1.009$. The bending stress distributions on the two surfaces at the three cross sections along the longitudinal direction ($x/L=0$, 1/4, 1/2) are shown in Fig. 5, in which the nominal stress $\sigma_0=6M_0/t_1^2$. At the supporting end, only the strip is burdened the almost bending moment. On the other hand, the bending stress spreads out over entire parts of strip and stiffener near the center of the span. Figure 6 shows the comparison of bending stress distribution along the z-axis between the numerical results and those of beam theory at the centers of the span and width ($x=L/2$, $y=0$). The bending stress distribution at this part agrees very well with that of theory. In contrast, the bending stress along the width shows some irregular distribution due to the connection of the stiffener and coarse mesh at the adhered region.

Figure 7 illustrates the shear stress contours on the adhered surface between the strip and the stiffener, in which the regions of shear stress τ greater than the theoretical nominal shear stress $\tau_0=0.376$ MPa at the supported ends are shaded, when the strip was applied with uniformly distributed load $p=0.01$ MPa. The shear stress distribution is obtained by averaging those of four Gauss points and taken to be the shear stress at the center of each element. The shear stress is concentrated at the edge of the adhered surface.

3.2 Simply supported isotropic plate with various stiffeners

Next, simply supported isotropic rectangular plates of aspect ratio $a/b=2.0$ with three types of stiffeners under uniform pressure $p=0.01$ MPa are considered to compare the different stress distributions due to the difference in cross-sectional shapes of stiffeners, as shown in Fig. 8. The three stiffeners are assumed to have the same thickness and the same bending stiffness. Quarter regions of isotropic stiffened plates are subdivided into 90 elements and 326 nodes in model (a), and into 102 elements and 366 nodes in models (b) and (c), because of symmetry. The material properties of the plate and the stiffeners

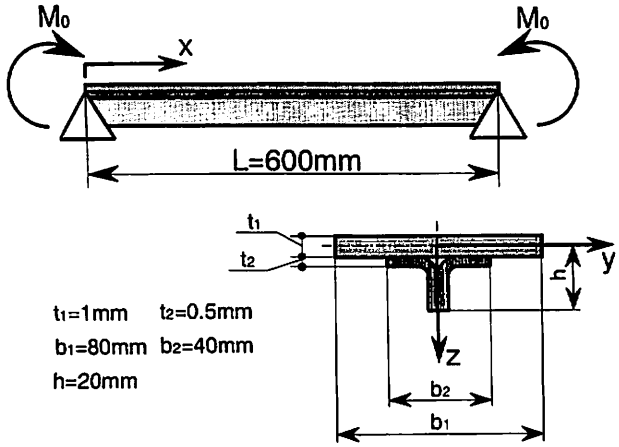

Fig. 4 Simply supported strip with T-type stiffener under uniform bending

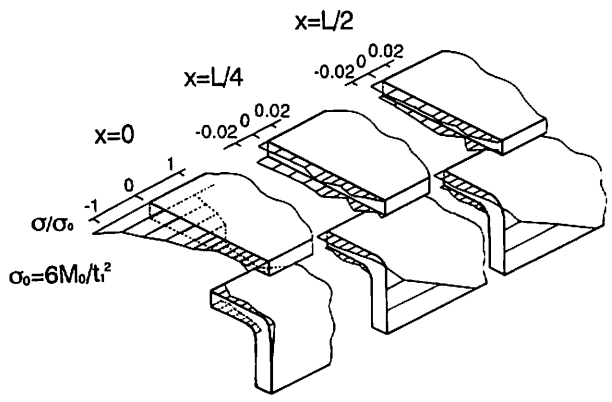

Fig. 5 Bending stress distribution on the surface along the strip

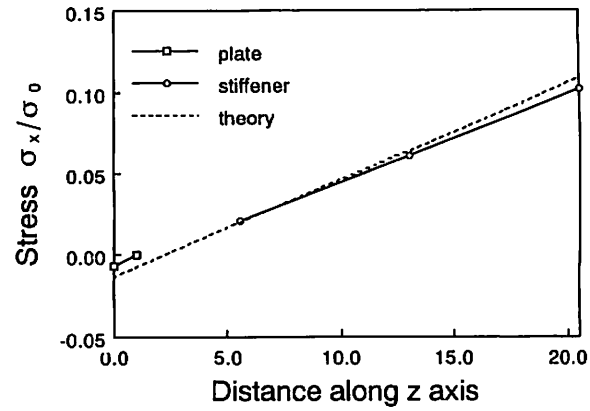

Fig. 6 Bending stress distribution along z-axis at centers of span and width

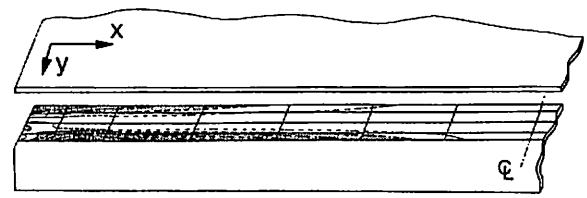

Fig. 7 Shear stress contours on adhered surface

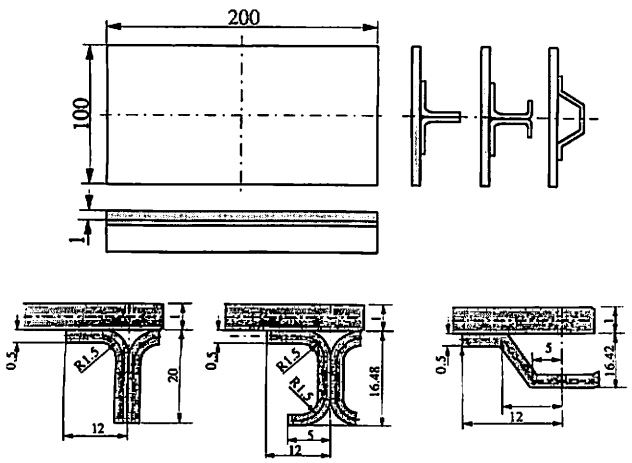

Fig. 8 Simply supported isotropic plates with stiffeners

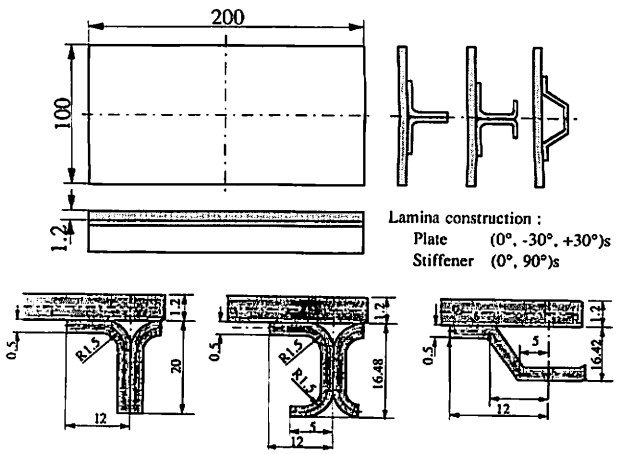

Fig. 10 Simply supported laminated composite plates with stiffeners

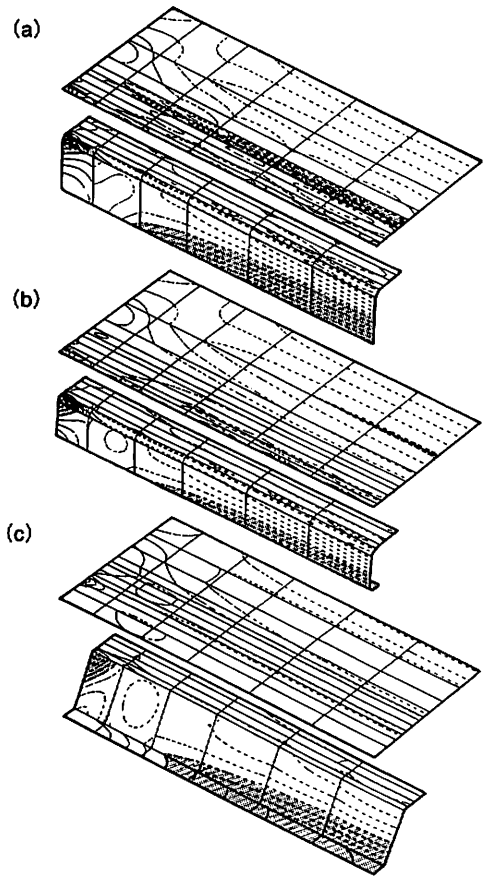

Fig. 9 The von Mises stress contours on surfaces of plates and stiffeners

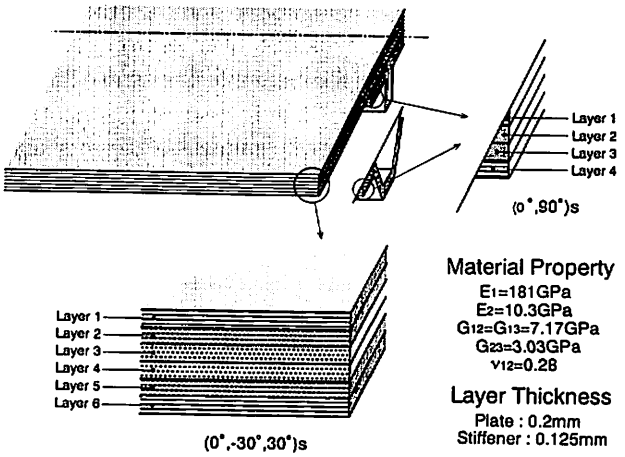

Fig. 11 Layer constructions of plate and stiffener

are assumed to be $E=200$ GPa and $\nu=0.25$.

The von Mises stress distributions on the surfaces of the plate and the stiffener are illustrated for each model in Fig. 9, in which the regions of stress greater than 10 MPa are shaded. In model (a), stress concentration on the plate surface near the end of the adhered region can be observed, but, the concentration is reduced in models (b) and (c). The stress distributions on the stiffener surfaces show some concentration at the center of edges and the roots of stiffener connections with the plate at the supported ends. The degree of concentration is lower in models (b) and (c) than in model (a).

3.3 Simply supported plates of laminated composite with stiffeners

Figures 10 and 11 show numerical models of simply supported composite plates with three types of stiffeners and their layer constructions. The structural model consists of graphite-epoxy (T 300/5208) as[6]

$E_L=181$ GPa, $E_T=10.3$ GPa,

$G_{LT}=G_{LH}=7.17$ GPa, $G_{TH}=3.03$ GPa, $\nu_{LT}=0.28$,

where the subscripts L, T and H represent the properties in the longitudinal and lateral directions of fiber, and in the thickness direction. Symmetric layer construction with respect to the midsurface, six layers of $[0°, -30°, 30°]_s$ in the plate and four layers of $[0°, 90°]_s$ in the stiffener are assumed, as shown in Fig. 11. The Tsai-Wu quadratic failure criterion is assumed to compare the stress distributions of each layer of plate and stiffener as

$$F_{LL}\sigma_L^2+2F_{LT}\sigma_L\sigma_T+F_{TT}\sigma_T^2+F_{SS}\tau_{LT}^2+F_L\sigma_L+F_T\sigma_T=1,$$

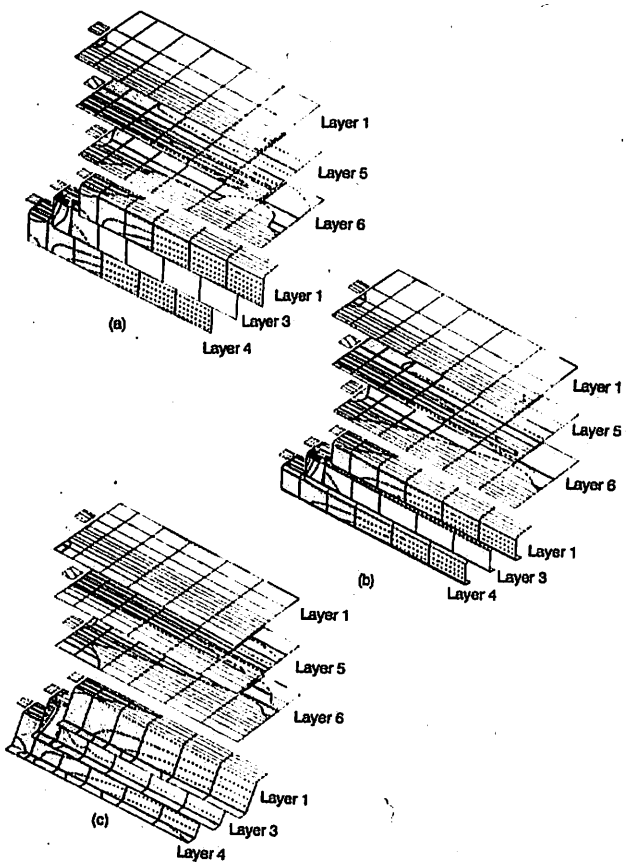

Fig. 12 Contours of quadratic failure criterion values on each layer surface

(24)

where F_{LL}, F_{TT}, F_{LT}, F_{SS}, F_L and F_T denote the constants given from the material strength of a unidirectional fiber-reinforced plate. The material constants of graphite-epoxy are given as[6]

$F_{LL}=0.4444(\mathrm{GPa})^{-2}$, $F_{LT}=-3.360(\mathrm{GPa})^{-2}$,
$F_{TT}=101.6(\mathrm{GPa})^{-2}$, $F_{SS}=216.2(\mathrm{GPa})^{-2}$,
$F_L=0$, $F_T=20.93(\mathrm{GPa})^{-1}$.

Failure will occur when Eq.(24) is satisfied at each layer of the plate and the stiffener.

86 A quarter region of the model is subdivided the same as in the previous examples. Figure 12 illustrates the distribution of the Tsai-Wu criterion values at the surface of each layer of the three stiffeners. The quadratic failure criterion values in the shaded region are positive in the figures. In model (a), the failure criterion values at the top edge and connecting root of the stiffener are greater than one. In all models, the fifth layer of plates have a high quadratic failure value. On the other hand, the failure criterion values at the stiffener edges are lower in models (b) and (c) than in model (a).

5. Concluding Remarks

In this paper, an integral-type of isoparametric shell connection element is proposed to represent the connectivity condition exactly at the adhered region using the penalty function method, and the finite element technique for analyzing the adhesive plate and shell structures is formulated. Then, the proposed technique is applied to the analysis of built-up structures such as the isotropic and laminated composite plates with several kinds of stiffeners. The numerical results show the validity of the proposed technique. Moreover, it is noted that the finite element analysis suggested here is applicable to shell built-up structures without any modification of the formulation.

References

(1) Bathe, K.J. and Chaudhary, A., A Solution Method for Planar and Axisymmetric Contact Problems, International Journal for Numerical Methods in Engineering, Vol. 21 (1985), p. 65.

(2) Chen, H.-W. and Tsai, P., Finite Element Analysis of Elastodynamic Sliding Contact Problems with Friction, Computers and Structures, Vol. 24 (1986), p. 925.

(3) Oden, J.T. and Kikuchi, N., Finite Element Methods for Constrained Problems in Elasticity, International Journal for Numerical Methods in Engineering, Vol. 18 (1982), p. 701.

(4) Kanto, Y. and Yagawa, G., A Dynamic Contact Buckling Analysis by the Penalty Finite Element Method, International Journal for Numerical Methods in Engineering, Vol. 29 (1990), p. 755.

(5) Hu, H.-T., Influence of Shell Geometry on Buckling Optimization of Fiber-Composite Laminate Shells, Proc. of the 32nd AIAA/ASME/ASCE/AHS/ASC Structures, Structural Dynamics and Material Conference, (1991), p. 284.

(6) Tsai, S.W. and Hahn, H.T., Introduction to Composite Materials, (1980), Technomic Publishing, Westport.